



## Density-Functional Tight-Binding for Platinum Clusters and Bulk: Electronic vs Repulsive Parameters

Ka Hung Lee,<sup>1,2</sup> Van Quan Vuong,<sup>1,2</sup> Victor Fung,<sup>3</sup> De-en Jiang,<sup>3</sup> Stephan Irle<sup>1</sup>

<sup>1</sup>Bredesen Center for Interdisciplinary Research and Graduate Education, University of Tennessee, Knoxville, TN 37996, U.S.A.

<sup>2</sup>Computational Sciences and Engineering Division and Chemical Sciences Division, Oak Ridge National Laboratory, Oak Ridge, TN 37831, U.S.A.

<sup>3</sup>Department of Chemistry, University of California, Riverside, CA 92521, U.S.A.

### ABSTRACT

We present a general purpose Pt-Pt density-functional tight-binding (DFTB) parameter for Pt clusters as well as bulk, using a genetic algorithm (GA) to automatize the parameterization effort. First we quantify the improvement possible by only optimizing the repulsive potential alone, and second we investigate the effect of improving the electronic parameter as well. During both parameterization efforts we employed our own training set and test sets, with one set containing ~20,000 spin-polarized DFT structures. We analyze the performance of our two DFTB Pt-Pt parameter sets against density functional theory (DFT) as well as an earlier DFTB Pt-Pt parameters. Our study sheds light on the role of both repulsive and electronic parameters with regards to DFTB performance.

Notice: This manuscript has been authored by UT-Battelle, LLC, under Contract no. DE-AC05-00OR22725 with the U. S. Department of Energy. The United States Government retains and the publisher, by accepting the article for publication, acknowledges that the United States Government retains a nonexclusive, paid-up, irrevocable, worldwide license to publish or reproduce the published form of this manuscript, or allow others to do so, for United States Government purposes. The Department of

Energy will provide public access to these results of federally sponsored research in accordance with the DOE Public Access Plan (<http://energy.gov/downloads/doe-public-access-plan>).

## INTRODUCTION

Platinum (Pt) is a rare metal that has long been known and used for their catalytic properties in both heterogenous and homogenous environments [1–4]. Countless computational catalysis studies of platinum and other transition metals have been performed extensively using first principles density functional theory (DFT) or *ab initio* methods, known for their high level of accuracy when compared to experiment. Because of the limits imposed by the high computational cost for these methods, theoretical mechanistic studies have largely been limited to either clusters of sizes up to ~100 atoms or periodic surface systems using idealized structures derived from bulk structures [1,5–9]. Given the increasing interest in platinum for pharmaceutical and biological applications as well as in clusters [10,11] a rapid evaluation of Pt clusters and bulk systems is highly desirable for researchers wishing to complement experimental work with theoretical calculation results. Efficient classical alternatives to quantum chemical calculations exist for the theoretical description of chemical reactions, such as the embedded atom model (EAM) [12], however these methods lack predictive capabilities and/or sufficient accuracy due to their neglect of electronic structure, essential for the theoretical description of catalytic cycles.

The computationally efficient, yet still theoretically rigorous methodology known as density-functional tight-binding (DFTB) provides a third alternative to acquiring accurate results with reasonably fast time to solution. Although the approach itself is an approximation to DFT, providing only a two-center approximation to atomic interaction as well as utilizing only a minimal basis set, DFTB (namely the second-order variant of DFTB, or DFTB2) has been proven to produce highly accurate results for transition metal oxides, transition metals, and transition metal alloys [13–18]. We note that the DFTB2 formalism [19,20] does not require the computation of Hubbard derivatives since they are only utilized in the third-order variant of DFTB, or DFTB3 [21].

A previous Pt-Pt DFTB2 parameter set was developed by Shi [17] utilizing the “hotbit” code [22] in combination with DFT. In the development of these parameters, which followed a traditional optimization strategy, the local density approximation (LDA) was used to generate DFTB2 electronic parameters, while the repulsive potentials were derived by fitting structures and energetics to DFT reference data using the generalized gradient approximation (GGA) functional of Perdew, Burke, and Ernzerhof (PBE) [23]. Their parameter set was meant primarily for studying Pt-Ru nanoclusters. Our overall goal in this work is to develop a general-purpose Pt-Pt parameter for Pt clusters as well as bulk, using a genetic algorithm (GA) to automatize the parameterization effort. First, we quantify the improvement possible by only optimizing the repulsive potential alone, and second, we switch out the electronic local density approximation (LDA)-based parameter from Shi with our own PBE-based electronic DFTB2 parameter. During both parameterization efforts we employed our own training set and test sets. We then analyze the performance of our two DFTB2 Pt-Pt parameter sets against DFT as well as the original parameters from Shi.

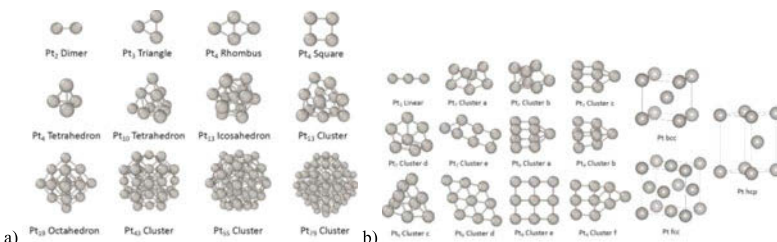
## PARAMETERIZATION STRATEGY

For this study, we have generated two new parameter sets for Pt-Pt interactions. We employed a genetic algorithm (GA)-based program “DFTBparaopt”, previously employed for the development of the ob2^0.3 organic set for long-range corrected-DFTB2 [24]. Two sets of properties were used for training the repulsive parameters, namely energies and geometries, of which the forces of equilibrated and perturbed (unequilibrated), structures could be obtained. Our scoring function  $f^{core}$  follows closely the formalism described by Vuong with  $f^{core}$  being defined as:

$$f^{score} = \sum_{i \in equi} W_{at,i} |F_{at,i}^{ref} - F_{at,i}^{DFTB}|^2 + \sum_{i \in equi} W_{f,i} \sum_{j \in 3N_i} |F_{i,j}^{DFTB}|^2 \\ + \sum_{i \in pert} W_{f,i} \sum_{j \in 3N_i} |F_{i,j}^{ref} - F_{i,j}^{DFTB}|^2 \quad (1),$$

where  $W_{at,i}$  and  $W_{f,i}$  are weight factors of  $i$ th atomization energy and  $i$ th force of structure for equilibrated (equi) and perturbated (pert) structures, respectively.

For this study, only trained parameters with lowest scores have been chosen for evaluation. Figure 1 illustrates the structures used for the training and small test sets, whereas Table S1 in the Supporting Information lists the structures, atomization energies, and atomization energy weights used for parameterizing Pt-Pt. Table S1 also lists the weight of forces of equilibrated structures and perturbed structures used for training. The settings shown in this Table for eLDA and ePBE contain values of weight factors found from the lowest scoring choices. For the  $\text{Pt}_2$  dimer, perturbed geometries were created by stretching and compressing the equilibrated Pt-Pt bond. For  $\text{Pt}_4$  and  $\text{Pt}_{10}$  tetrahedron structures, stretched and compressed geometries were created by multiplying a scalar



factor of 0.90, 0.95, 1.05, and 1.10 to the atomic positions of the equilibrated Pt<sub>4</sub> and Pt<sub>10</sub> structures.

**Figure 1.** DFT reference sets used for a) training (the training set) and b) testing (the small test set).

The first parameter, named eLDA for this study, utilized Shi's LDA-based electronic parameter but had their repulsive parameters retrained. The purpose of this first parameter set is to monitor the effects the repulsive training has on DFTB performance in general. The second parameter, named ePBE for this study, utilizes a GGA-based electronic parameter instead of LDA with compression radii taken from the "auorg" DFTB parameter set for gold, with the exception of the compression radius of the 6p-orbital, which was set at 6.5  $\text{Å}$ , consistent with the compression of the 6s and 5d

orbitals [13]. For both parameter sets eLDA and ePBE, the repulsive parameters were fully optimized individually by the GA-based code.

The total atomization energies  $E_{at}$  of platinum clusters was derived from various non-spin polarized and neutral platinum clusters ( $Pt_n^0$ ) that were computed using VASP 5.4 with PBE and an energy cutoff of 550 eV [25]. For all DFT reference structures, the forces were converged within 1 meV/Å. The Gaussian smearing scheme was used throughout the study with a smear broadening of 0.05 eV. The total energies obtained from VASP were extrapolated to zero smearing energies ( $E_0$ ). The total atomization energy of DFT structures was derived from the binding energy per atom of individual clusters  $E_{binding}$  as defined in the equation below:

$$E_{binding} = [E(Pt_n) - n \times E(Pt_1)]/n \quad (2),$$

$$E_{at} = -n \times E_{binding} \quad (3),$$

where  $n$  is the number of atoms,  $E(Pt_n)$  is the total energy of an  $n$ -numbered cluster, and  $E(Pt_1)$  is the total energy of an isolated free Pt atom without spin polarization (-0.15 eV). With the exception of the isolated free atom, periodic bulk structures (bulk face-centered cubic, or fcc, body-centered cubic, or bcc, and hexagonal cubic packing, or hcp Pt), and the linear  $Pt_3$  molecule, the periodic boundary box size for all  $Pt_n$  clusters was 20 Å x 20 Å x 20 Å to ensure the proper isolation of clusters in vacuum within 1 meV. Additionally, symmetry was not used during optimization of isolated clusters. The isolated free atom was calculated using a broken symmetry box with a 19 Å x 20 Å x 21 Å periodic boundary box to ensure the proper occupancy of orbitals up to 0.05 eV of smear broadening.

Regarding sampling of the Brillouin zone, a 1 x 1 x 1 k-point selection was used in the case of isolated clusters, whereas an 11 x 11 x 11 k-point mesh was selected for bulk fcc and bcc structures, and an 11 x 11 x 9 k-point mesh was used for bulk hcp. For DFTB, all calculations were performed using DFTB+, version 18.2 [26]. The electronic temperature for all DFTB calculations was set to 300.0 K to avoid potential convergence problems from self-consistent charge convergence in DFTB2, thus the total Mermin free energy was used when compared to DFT results. The default force criteria of  $10^{-4}$  a.u. on DFTB+ has been used for computing DFTB structures with an SCC tolerance set at  $10^{-9}$  a.u.

The repulsive potential in both parameter sets is expressed by a combination of an exponential component near the origin of the atom and a 4<sup>th</sup> order spline function away from the atom. By using a series of optimized knots that determine the range of the splines (see Table S2), the 4<sup>th</sup> order spline functions (see Figure S1) were fitted using the least mean squared algorithm developed by Gaus [27], and solved using the GA procedure in DFTBparaopt. As DFTB often shows systematic overbinding in covalent bonds, we had shifted our atomization energies by +0.148 eV/atom, the energy of the isolated free Pt atom, during our training only.

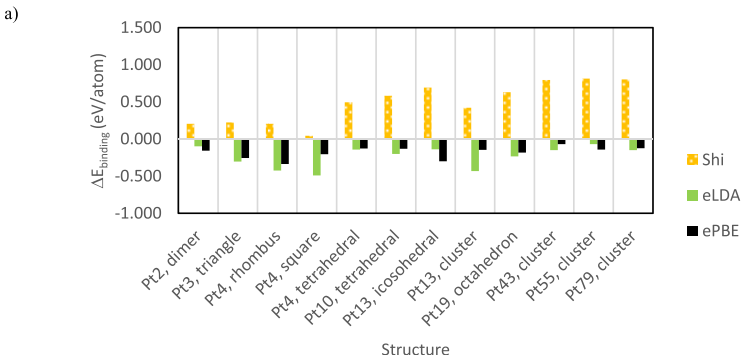
## RESULTS AND DISCUSSION

### Energy performance for training and small test set

To compare the performance of our new parameters with those by Shi, we first analyze the results of the training and small test sets in terms of binding energies (as

defined in Eq. 2) relative to non-spin-polarized PBE ( $\Delta E_{\text{binding}}$ ) as shown in Figure 2a and 2b. The small test set includes periodic Pt structures (fcc, bcc, and hcp) and 12 small clusters ( $\text{Pt}_3$ ,  $\text{Pt}_7$ ,  $\text{Pt}_9$ ), totaling 15 structures. The root mean square deviation (RMSD) of binding energies for non-spin polarized clusters was 0.56 eV/atom (Shi), 0.27 eV/atom (eLDA), and 0.20 eV/atom (ePBE), respectively for the training set, and 0.59 eV/atom (Shi), 0.41 eV/atom (eLDA), 0.23 eV/atom (ePBE), respectively for the small test set.

In both instances our current parameters have been faring better than the original parameters from Shi. The poorest performance from the parameters of Shi comes from the description of bulk and large cluster binding energies. However, in our new parameters, this issue has largely been alleviated both in bulk and in large clusters. While the parameter of Shi was able to reproduce bulk binding energies of bulk much closer to that of DFT after lattice relaxation, it had sacrificed its performance in geometry (see Table 1 in the following section). This inconsistent improvement in bulk and surface energies despite the changes to DFTB geometries can be explained by the empirical tuning of the orbital energy of the d valence orbital  $\epsilon_d$  that was carried out in their study. As pointed out by Shi, such manual refinements, if done properly, can lead to optimal results. While such “tuning” had not been applied in this work, more sophisticated approaches to DFTB parameterization suggests that an additional optimization of DFTB electronic parameters could indeed improve the overall quality of DFTB parameters [18,24].



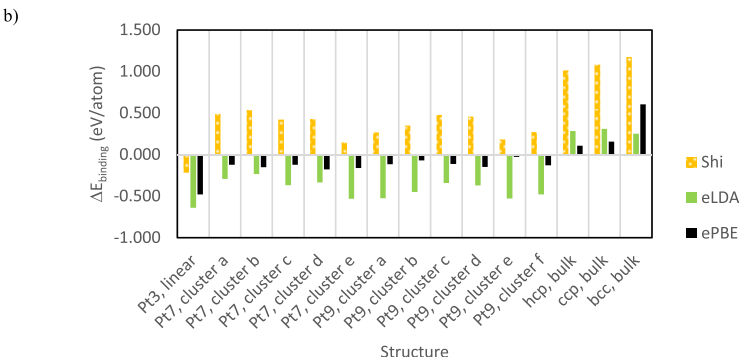


Figure 2. Performance of DFTB2 binding energies relative to PBE ( $\Delta E_{\text{binding}}$ ) for the a) training set and b) small test set from PBE geometries.

#### Geometry performance for training and small test set

Considering the performance of the parameters for geometries, the comparison between DFTB and PBE structures is shown in Figures 3a and 3b. For clusters, we compared structures using mean absolute deviation (MAD) of Pt-Pt bond distances relative to PBE geometries (bond MAD) while bulk lattice parameters were used to compare bulk Pt systems also optimized using PBE (see Table 1). In our study it has been found that structures under 0.2 Å bond MAD in clusters generally retain their original DFT geometry as shown in Figure S2. In the case of the Pt<sub>4</sub> tetrahedron, the structure using the parameters from Shi could not retain its original geometry and adopts a square configuration. Overall, the RMSD value for the bond MAD of Pt cluster is about 0.18 Å (Shi), 0.08 Å (eLDA), and 0.03 Å (ePBE), respectively for the training set and 0.14 Å (Shi), 0.08 Å (eLDA), and 0.03 Å (ePBE), respectively for the small test set. Generally, both eLDA and ePBE were able to reduce the error relative to the parameters of Shi, in particular the error found in medium to large clusters. However, of the two parameters (ePBE and eLDA), only ePBE was able to resolve all major geometrical problems when compared to PBE optimized structures.

This consistent improvement in geometries is similarly reproduced in bulk structures with ePBE being able to reproduce values much closer to DFT than the parameters by Shi. This showcases our new ePBE parameter has the ability to reproduce not just for a variety of Pt cluster sizes, but also for bulk Pt. Although eLDA was unable to reproduce bulk hcp structures like ePBE, its performance for other geometries are still significantly better than those from Shi as noticeable from the lower RMSD value when it comes to the training and small test sets as well as from fcc and bcc geometries.

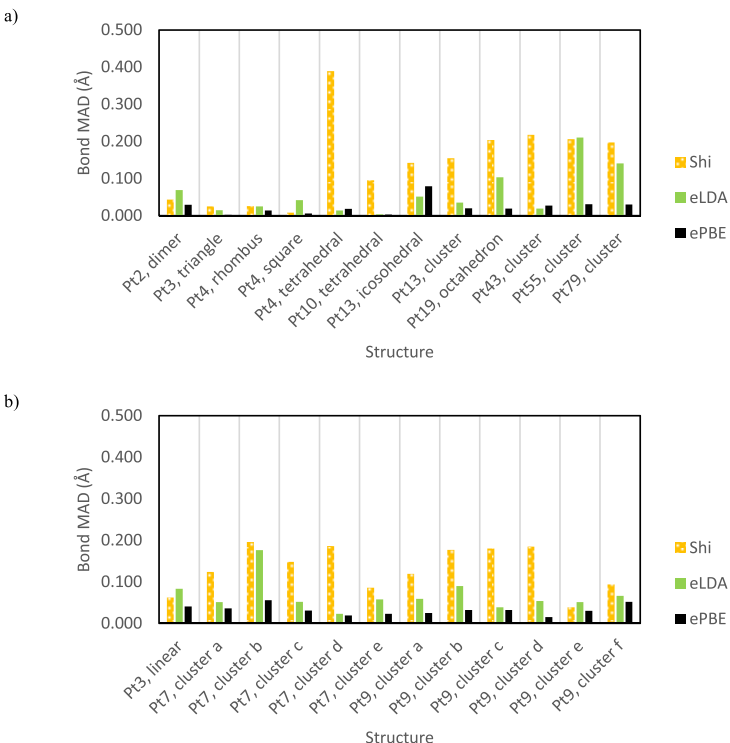


Figure 3. Performance of DFTB2 bond distances relative to PBE geometries for the a) training set and b) small test set.

Table 1. The lattice parameters and binding energies of Pt hcp, fcc, and bcc structures.

hcp	PBE	PBE (published)	Reference (experimental)	Shi	eLDA	ePBE
a/Å	2.76	2.72 <sup>a</sup>		2.92	not hcp	2.82
b/Å	2.76			2.92		2.82
c/Å	4.76	4.68		4.81		4.82
c/a	1.73	1.72 <sup>a</sup>		1.65		1.71
$\alpha/^\circ$	90.0			90.0		90.0
$\gamma/^\circ$	120.0			120.0		120.0
$E_{\text{binding}}/\text{eV}\cdot\text{atom}^{-1}$ (atom, no spin)	-5.90			-5.56		-5.82
$E_{\text{binding}}/\text{eV}\cdot\text{atom}^{-1}$ (atom, with spin)	-5.42			N/A		-4.32
fcc	PBE	PBE (published)	Reference (experimental)	Shi	eLDA	ePBE
a/Å	3.97	3.98 <sup>b</sup>	3.91 <sup>b</sup>	4.14	4.06	4.05
$\alpha/^\circ$	90.0	90.0		90.0	90.0	90.0
$E_{\text{binding}}/\text{eV}\cdot\text{atom}^{-1}$ (atom, no spin)	-5.97			-5.63	-5.73	-5.86
$E_{\text{binding}}/\text{eV}\cdot\text{atom}^{-1}$ (atom, with spin)	-5.49	-5.50 <sup>b</sup>	-5.87 <sup>b</sup>	N/A	N/A	-4.36 <sup>c</sup>

with spin)						
bec	PBE	PBE (published)	Reference (experimental)	Shi	eLDA	ePBE
a/Å	3.16			3.35	3.24	3.06
$\alpha^{\circ}$	90.0			90.0	90.0	90.0
$E_{\text{binding}}/\text{eV}\cdot\text{atom}^{-1}$ (atom, no spin)	-5.97			-5.49	-5.69	-5.51
$E_{\text{binding}}/\text{eV}\cdot\text{atom}^{-1}$ (atom, with spin)	-5.49			N/A	N/A	-4.01 <sup>c</sup>

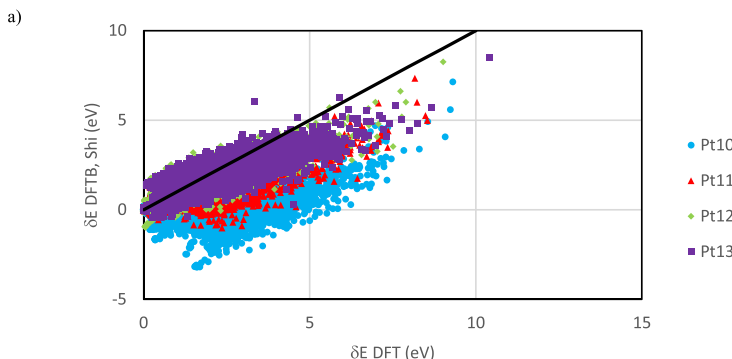
<sup>a</sup>Ref. [28].  
<sup>b</sup>Ref. [29] uses spin polarized free atom to compute the binding energy of bulk Pt and corrected experimental values from Lejaeghere [30].  
<sup>c</sup>The difference in energy is due to the energy difference between non-spin and spin-polarized Pt atom in DFTB, which is around ~1.5 eV with the spin-polarized atom (Pt electron configuration: 5d<sup>6</sup>6s<sup>1</sup>) being lower in energy.

### **Energy and geometry performance for large test set**

A more comprehensive test was conducted using ~20,000 Pt<sub>10</sub> to Pt<sub>13</sub> clusters from the work of Fung [31]. Relative isomer energies and geometries were used to gauge the performance of DFTB relative to PBE. For relative energies, the reference point used is the total energy of lowest energy cluster from each size of Pt.

In Figure 4 the energy performance is visualized, of which the ideal case of  $\delta E$  DFTB equals  $\delta E$  PBE being represented by a bolded line with a slope of 1. Table S3 summarizes the MAD, RMSD, mean signed deviation (MSD), max deviations (MAX), and  $R^2$  of  $\delta E$  with Figure S3 providing a graphical representation of the relative energy distribution from PBE found in Figure 4 as  $\Delta E$ .

In terms of  $R^2$ , both eLDA and ePBE are better correlated than those found from Shi. Similarly, only 59% of Pt clusters were located within 1 eV (36% within 0.5 eV) of PBE when using the parameters from Shi, compared to 70% using eLDA (47% within 0.5 eV), and 86% using ePBE (52% within 0.5 eV). Based on their relative isomer energies, the general performance of eLDA and ePBE are shown to be substantially improved from Shi with average MAD isomer energy across all sizes being 1.16 eV (Shi), 0.91 eV (eLDA), and 0.54 eV (ePBE), respectively, and average RMSD isomer energy across all sizes being 1.37 eV (Shi), 1.03 eV (eLDA), and 0.65 eV (ePBE), respectively.



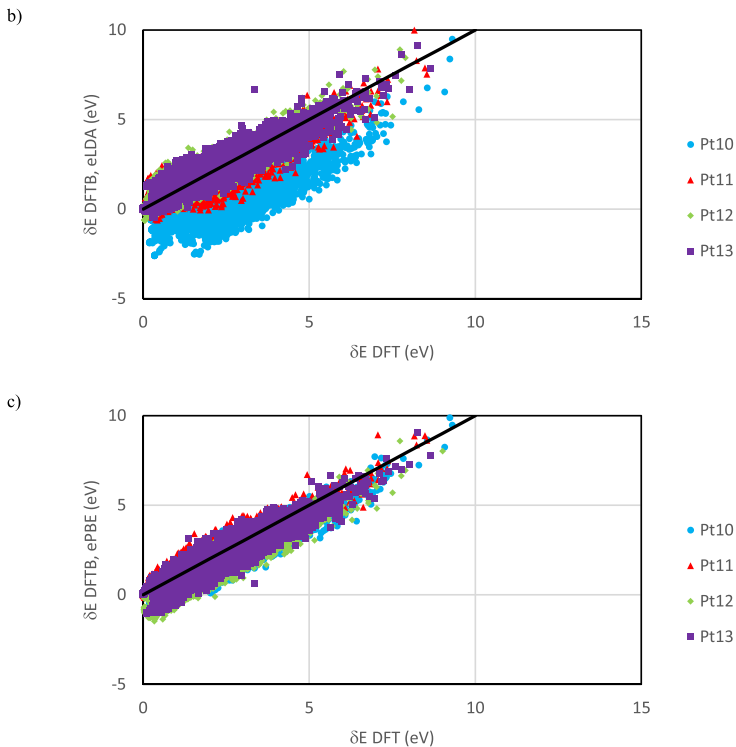


**Figure 4. Performance of DFTB2 relative energies when compared to PAW-PBE; a) Shi, b) eLDA, and c) ePBE.**

When comparing optimized geometries of Pt, substantial improvements can be seen from both new parameters (see Figure 5), similar to improvements shown from the training and small test sets. The average bond distance MAD values for all clusters sizes in were 0.17 Å, 0.09 Å, and 0.05 Å, respectively for Shi, eLDA, and ePBE. Compared to just 2% of the roughly 20,000 DFT basin-hopping structures being within 0.1 Å bond distance MAD, LDA elec. can reproduce up to 73% of all reference structures. Similarly, PBE elec. was able to reproduce 98% of all reference structures within 0.1 Å bond distance.

As the training set were not originally intended to reproduce spin-polarized DFT results, the level of accuracy found in non-spin polarized DFTB was quite unexpected. However, this trait does suggest that spin polarization might not play as significant of a role when it comes to describing the relative energies of similarly sized Pt clusters when it comes to DFTB.

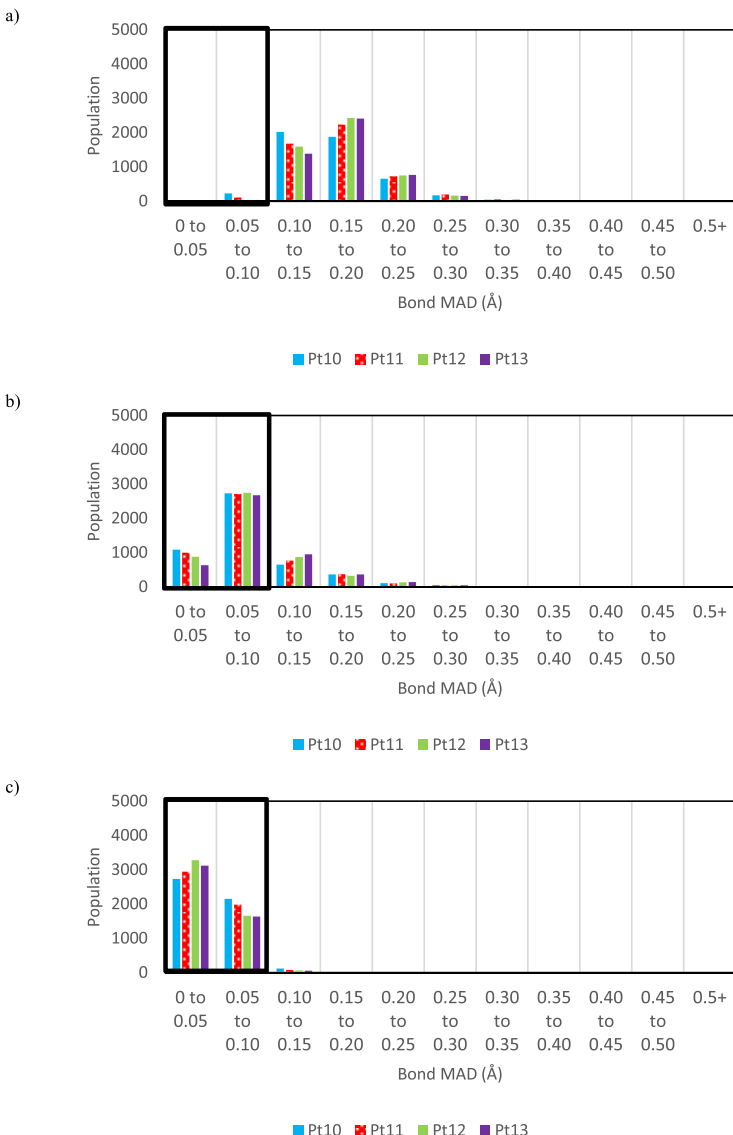


Figure 5. Population distribution of bond MAD for a) Shi, b) eLDA, and c) ePBE. The bolded box represents energies within 0.1 Å of PBE.

## CONCLUSION

In this study, we have developed general purpose density-functional tight-binding parameters at the DFTB2 level of theory for Pt-Pt interactions in clusters and bulk, and have validated energies and geometries in newly designed training and small and large tests sets. Our automatic parameterization scheme was able to derive parameters that generally improve both the energetics and geometries of Pt clusters. For general purpose usage, we have found both eLDA and ePBE parameter sets to be suitable for reproducing DFT-quality clusters and bulk energies and geometries, with ePBE generally providing better performance, in particular, for bulk and large clusters when compared against PBE-derived reference data. The additional comparison between DFTB and a spin-polarized DFT basin-hopping search further suggests that the new parameters can be applied for DFT-level structural searches for small Pt clusters, providing geometries well within 0.1 Å Pt-Pt bond MAD.

While the change in electronic parameters from LDA-based parameters to GGA-based electronic parameters was found to have a significant impact on the overall quality of DFTB parameters, the comparison between eLDA and those of Shi, highlights the significance of the repulsive parameters. As the electronic parameters themselves had not been rigorously retrained or optimized in our study, our results for eLDA suggest that the careful training of repulsive potentials alone could partially compensate for the lack in quality in Pt parameters but are insufficient if one desires parameters of higher quality, measured by agreement with PBE reference data. For better performing parameters, ePBE suggests that both electronic and repulsive parameters would need to be retrained or altered, a conclusion that was shared in the papers of Vuong [24], as well as Bossche [18].

## ACKNOWLEDGMENTS

K.H.L. and V.Q.V were supported by an Energy Science and Engineering Fellowship by the Bredesen Center for Interdisciplinary Research and Graduate Education at the University of Tennessee, Knoxville. This work was sponsored by the U.S. Department of Energy, Office of Science, Office of Basic Energy Sciences, Chemical Sciences, Geosciences, and Biosciences Division. This research used resources of the National Energy Research Scientific Computing Center, a DOE Office of Science User Facility supported by the Office of Science of the U.S. Department of Energy under contract no. DE-AC02-05CH11231.

## REFERENCES:

- [1] Y. H. Chin, C. Buda, M. Neurock, and E. Iglesia, *J. Catal.* **283** (1), 10–24 (2011).
- [2] V. N. Korchak, M. V. Grishin, M. Y. Bykhovskii, A. K. Gatin, V. G. Slutskii, V. A. Kharitonov, S. A. Tsygannov, and B. R. Shub, *Russ. J. Phys. Chem. B* **11** (6), 932–936 (2017).
- [3] J. A. Kurzman, L. M. Misch, and R. Seshadri, *Dalt. Trans.* **42** (41), 14653–14667 (2013).
- [4] A. Galván, J. Calleja, F. J. Fañanás, and F. Rodríguez, *Angew. Chemie - Int. Ed.* **52** (23), 6038–6042 (2013).
- [5] O. E. Polozhentsev, V. K. Kochkina, V. L. Mazzalova, and A. V. Soldatov, *J. Struct. Chem.* **57** (7), 1477–1484 (2016).
- [6] B. Hamad, Z. El-Bayyari, and A. Marashdeh, *Chem. Phys.* **443**, 26–32 (2014).
- [7] D. Xenides and G. Maroulis, *J. Comput. Methods Sci. Eng.* **5**, 1–9 (2005).
- [8] L. Liu and A. Corma, *Chem. Rev.* **118** (10), 4981–5079 (2018).

- [9] S. Heiles and R. L. Johnston, *Int. J. Quantum Chem.* **113** (18), 2091–2109 (2013).
- [10] M. Mauro, A. Aliprandi, D. Septiadi, N. S. Kehr, and L. De Cola, *Chem. Soc. Rev.* **43** (12), 4144–4166 (2014).
- [11] T. Banerjee, P. Dubey, and R. Mukhopadhyay, *Biochimie* **94** (2), 494–502 (2012).
- [12] M. I. Mendelev, S. Han, D. J. Srolovitz, G. J. Ackland, D. Y. Sun, and M. Asta, *Philos. Mag.* **83** (35), 3977–3994 (2003).
- [13] J. Cuny, N. Tarrat, F. Spiegelman, A. Huguenot, and M. Rapacioli, *J. Phys. Condens. Matter* **30** (30), 303001 (2018).
- [14] J. Kullgren, M. J. Wolf, K. Hermansson, C. Köhler, B. Aradi, T. Frauenheim, and P. Broqvist, *J. Phys. Chem. C* **121** (8), 4593–4607 (2017).
- [15] G. Dolgonos, B. Aradi, N. H. Moreira, and T. Frauenheim, *J. Chem. Theory Comput.* **6** (1), 266–278 (2010).
- [16] G. Zheng, H. A. Witek, P. Bobadova-Parvanova, S. Irle, D. G. Musaev, R. Prabhakar, K. Morokuma, M. Lundberg, M. Elstner, C. Köhler, and T. Frauenheim, *J. Chem. Theory Comput.* **3** (4), 1349–1367 (2007).
- [17] H. Shi, P. Koskinen, and A. Ramasubramanian, *J. Phys. Chem. A* **121** (12), 2497–2502 (2017).
- [18] M. Van den Bossche, *J. Phys. Chem. A* **123** (13), 3038–3045 (2019).
- [19] M. Elstner, *Theor. Chem. Acc.* **116**, 316–325 (2006).
- [20] M. Gaus, Q. Cui, and M. Elstner, *Wiley Interdiscip. Rev. Comput. Mol. Sci.* **4** (1), 49–61 (2014).
- [21] M. Gaus, Q. Cui, and M. Elstner, *J. Chem. Theory Comput.* **7** (4), 931–948 (2011).
- [22] P. Koskinen and V. Mäkinen, *Comput. Mater. Sci.* **47** (1), 237–253 (2009).
- [23] P. E. Blöchl, *Phys. Rev. B* **50** (24), 17953–17979 (1994).
- [24] V. Q. Vuong, J. Akkarapattiakal Kuriappan, M. Kubillus, J. J. Kranz, T. Mast, T. A. Niehaus, S. Irle, and M. Elstner, *J. Chem. Theory Comput.* **14** (1), 115–125 (2018).
- [25] G. Kresse and D. Joubert, *Phys. Rev. B* **59** (3), 1758–1775 (1999).
- [26] B. Aradi, B. Hourahine, and T. Frauenheim, *J. Phys. Chem. A* **111** (26), 5678–5684 (2007).
- [27] M. Gaus, C. P. Chou, H. Witek, and M. Elstner, *J. Phys. Chem. A* **113** (43), 11866–11881 (2009).
- [28] S. Schönecker, X. Li, M. Richter, and L. Vitos, *Phys. Rev. B* **97** (22), 224305 (2018).
- [29] P. Janthon, S. Luo, S. M. Kozlov, F. Viñes, J. Limtrakul, D. G. Truhlar, and F. Illas, *J. Chem. Theory Comput.* **10** (9), 3832–3839 (2014).
- [30] K. Lejaeghere, V. Van Speybroeck, G. Van Oost, and S. Cottenier, *Crit. Rev. Solid State Mater. Sci.* **39** (1), 1–24 (2014).
- [31] V. Fung and D.-E. Jiang, *J. Phys. Chem. C* **121** (20), 10796–10802 (2017).